2-25-2008

Ab initio calculation of carbon clusters. II. Relative stabilities of fullerene and nonfullerene C_{24}

Wei An
University of Nebraska - Lincoln

Nan Shao
University of Nebraska - Lincoln, nshao@unomaha.edu

Satya S. Bulusu
University of Nebraska-Lincoln, sbulusu@iiti.ac.in

Xiao Cheng Zeng
University of Nebraska-Lincoln, xzeng1@unl.edu

Ab initio calculation of carbon clusters. II. Relative stabilities of fullerene and nonfullerene C_{24}

Wei An, Nan Shao, Satya Bulusu, and X. C. Zeng[a)]
Department of Chemistry, University of Nebraska-Lincoln, Lincoln, Nebraska 68588, USA

(Received 14 November 2007; accepted 14 December 2007; published online 25 February 2008)

Chemical stabilities of six low-energy isomers of C_{24} derived from global-minimum search are investigated. The six isomers include one classical fullerene (isomer 1) whose cage is composed of only five- and six-membered rings (5/6-MRs), three nonclassical fullerene structures whose cages contain at least one four-membered ring (4-MR), one plate, and one monocyclic ring. Chemical and electronic properties of the six C_{24} isomers are calculated based on a density-functional theory method (hybrid PBE1PBE functional and cc-pVTZ basis set). The properties include the nucleus-independent chemical shifts (NICS), singlet-triplet splitting, electron affinity, ionization potential, and gap between the highest occupied molecular orbital and the lowest unoccupied molecular orbital (HOMO-LUMO) gap. The calculation suggests that the neutral isomer 2, a nonclassical fullerene with two 4-MRs, may be more chemically stable than the classical fullerene (isomer 1). Analyses of molecular orbital NICS show that the incorporations of 4-MRs into the cage considerably reduce paratropic contributions from HOMO, HOMO-1, and HOMO-2, which are mainly responsible for the sign change in NICS from positive for isomer 1 (42) to negative (−19) for isomer 2, although C_{24} clusters satisfy neither $4N+2$ nor $2(N+1)^2$ aromaticity rule. Anion photoelectron spectra of four cage isomers, one plate, one monocyclic ring, and one tadpole isomer, as well as three bicyclic ring isomers are calculated. The simulated photoelectron spectra of mono- and bicyclic rings (with C_1 symmetry) appear to match the measured HOMO-LUMO gap (between the first and second band in the experimental spectra) [S. Yang *et al.*, Chem. Phys. Lett. **144**, 431 (1988)]. Nevertheless, the nonclassical fullerene isomers 3 and 4 apparently also match the measured vertical detachment energy (2.90 eV) reasonably well. These results suggest possible coexistence of nonclassical fullerene isomers with the mono- and bicyclic ring isomers of C_{24}^- under the experimental conditions. © *2008 American Institute of Physics*. [DOI: 10.1063/1.2831917]

I. INTRODUCTION

Classical fullerenes C_n are spherelike polyhedra incorporating exactly 12 pentagons and $(n/2-10)$ of hexagons.[1,2] A unique feature of these cage molecules is their transformation from normal carbon sp^2 trivalent bonds into a spherical framework via distortion while still remaining stable. The pentagons are needed for geometrical closure, whereas the hexagons are for maximizing the π-delocalization energy of these unsaturated molecules.[3] The stability of carbon fullerene stems from both geometric and electronic bonding factors. The (empirical) isolated-pentagon rule[4–6] (IPR) states that fullerenes with more isolated (nonadjoining) pentagons are energetically more favorable. The IPR implicates that framework with only five- and six-membered rings (5/6-MRs) is likely to occur spontaneously and to survive the simultaneous coalescence without losing individual identity. The IPR can explain the high stability of C_{60} fullerene structure whose 12 pentagons are completely surrounded by hexagons, as well as predict successfully the stable fullerenes with "magic number" $n=32$, 36, 50, 60, 70, 76, 78, and 84.[3–13] The IPR can be theoretically rationalized on both steric and π-electronic grounds. Fullerenes with three-, four-, and seven-membered rings (3-, 4-, and 7-MRs) are reasonably ruled out due to extra local steric strain and loss of π-delocalization. However, few theoretical studies have shown that nonclassical fullerenes, especially those containing 4-MRs, can compete with classical fullerenes in chemical stabilities.[14–21] We note that a nonclassical fullerene C_{62} containing a 4-MR has been synthesized and detected experimentally.[21]

There have been increasing research interests in small to medium-sized $(n=20-36)$ carbon clusters since the discovery of the C_{60}.[7–13,17,22–31] In our previous paper (Paper I[26]), we studied relative stabilities of various isomers of carbon cluster C_{20} using high-level *ab initio* methods. In that study, the bowl-shaped "fullerene fragment" corannulene was theoretically identified as the ground-state isomer of C_{20}, which has a lower energy than the (only) classical fullerene isomer of C_{20}. Indeed, the bowl-shaped isomer of C_{20} has been experimentally detected in photoelectron spectroscopy (PES) experiment.[8,13] The experiment provides a supporting evidence for the growth mechanism[32–37] of the so-called "pentagon road"[32] by which the formation of fullerenes from small carbon fragment can be realized via incorporation of pentagons through annealing ($\geqslant$1473 K), consistent with the IPR. This growth mechanism can explain the high yield of C_{60} production.[1,2] However, the so-called "fullerene road"[33]

a)Electronic mail: xczeng@phase2.unl.edu.

can also explain fullerene formation via ring→fullerene isomerization during the collisional heating (≥3740 K) process. In fact, small-sized carbon rings become more stable than the fullerene cage structures as the temperature is increased[26] and are commonly observed under the experimental condition.[28–31] Recently, a "shrinking hot giant road" which describes the self-assembled fullerene formation from chaotic hot carbon radicals under nonequilibrium conditions is proposed based on quantum mechanical molecular dynamics simulations within non-self-consisitent charge density functional tight binding approximation.[37]

Starting from C_{24}, previous theoretical calculations suggest that the classical fullerene cage is most likely the ground-state structure.[17,22–25] An intermediate carbon phase, "cubic graphite" which has a simple cubic lattice formed by C_{24} fullerene molecules and copolymerized by the square faces, has been characterized.[38] For its survival, an as-made fullerene should have certain degree of chemical stability with which the activation energy barrier for further chemical bonding with other identical or different-sized carbon clusters must be high enough to prevent fullerene from closure breaking. Accordingly, the intracluster covalent bonding must be strong enough or at least stronger than the cluster-cluster interaction. As for fullerenes containing four-membered rings (4-MRs), the stress induced by large curvature may be better released in C_{24} than in larger nonclassical fullerenes such as C_{40},[14,15] C_{52},[20] and C_{62},[21] so that nonclassical fullerene isomers of C_{24} can be energetically competitive.

In this paper (Paper II in this series), we report *ab initio* study of the relative chemical stabilities of six low-energy fullerene isomers of C_{24} and C_{24}^-. The identification of the candidate cage isomers was based on an extensive search for the low-lying C_{24} clusters using a global optimization technique coupled with the density-functional theory (DFT) method.

II. COMPUTATIONAL DETAILS

We performed a global search for the low-lying isomers of C_{24} using the basin-hopping (BH) method[39] combined with DFT geometric optimization which is implemented in the Car-Parrinello molecular dynamics (CPMD) program[40] and DMOL3 package.[41] Details of the basin-hopping method has been described elsewhere.[42] The Perdew-Burke-Ernzerhof (PBE) exchange and correlation functional was selected for the DFT calculation.[43] We obtained more than 100 neutral isomers of C_{24}, including both cage isomers and noncage isomers. Among them, the four lowest-lying isomers of C_{24} have cage structures.

We then carried out further geometry optimization for the four lowest-lying cage isomers and their anion C_{24}^- isomers using a hybrid exchange-correlation functional PBE1PBE (Ref. 43) and a large cc-pVTZ basis set[44] [Dunning's correlation consistent polarized valence triple zeta, contracted $[4s3p]$ plus polarization set $(2d1f)$], implemented in the GAUSSIAN03 software package.[45] Harmonic vibrational frequencies were also calculated to confirm that the optimized structures were local minima on the potential energy surface. We also computed several chemical/physical indices for characterizing their stabilities (using the PBE1PBE/cc-pVTZ level), including the singlet-triplet splitting (ΔE_{ST}), electron affinity (EA), ionization potential (IP), Gibbs free energy (0.5–3000 K), and nuclear independent chemical shift (NICS).[46–52]

For NICS analysis, we used the gauge-independent atomic orbital (GIAO) method[53,54] to evaluate natural localized molecular orbital (NLMO) contributions, and the canonical molecular orbital (CMO) method (implemented in the NBO 5.0 program)[55,56] to evaluate canonical MO contributions. The NICS analysis is useful to investigate the difference in aromaticity between the classical and nonclassical fullerene isomers.

III. RESULTS AND DISCUSSION

Using the BH/DFT method as a screening tool, we collected more than 100 isomers of C_{24}. Both BH-DMOL and BH-CPMD searches were performed. Structures of these isomers have either cage or noncage structures. We found that in the BH search, small-sized carbon clusters such as C_{24} have a tendency to open the cage and form multi-rings, which are also local minima. While the BH-DMOL search tends to generate noncage isomers, the BH-CPMD search tends to generate cagelike structures. Thus, the two approaches complement to each other in generating candidate isomers. Note that to enhance the speed of computation, we used a relatively smaller energy cutoff (25 Ry) for the BH-CPMD search and a smaller global-orbital-cutoff radius (4.0 Å) for the BH-DMOL search.

The energy rankings (calculated using DMOL3) for the top 30 low-energy isomers are given in Table I. We then used the PBE1PBE/cc-pVTZ method to reoptimize the top ten low-lying isomers, from which we identified four lowest-lying cage isomers (i.e., 1–4). For the purpose of comparison, we also included two noncage isomers, 5 and 6. Here, 5 is a plate isomer and 6 is a monocyclic-ring isomer.

A. Geometries

Structures of eleven C_{24} isomers are displayed in Fig. 1, where the bond types are solely determined by bond lengths. Isomers 1, 5, and 6 can be viewed as three prevailing structures, similar to the fullerene cage, bowl, and monocyclic-ring isomers of C_{20} (Paper I[26]). The three structural topologies are common to all small-sized carbon clusters. Cage isomers 2–4 and 7–11 are nonclassical fullerenes because of the inclusion of 4-MRs. Compared to 1, isomers 7 (0.39 eV), 8 (0.46 eV), 9 (0.51 eV), and two other cage isomers with high symmetry, 10 (1.32 eV, O_h) and 11 (5.19 eV, D_{2h}), have notably higher energies. The fullerenes containing

TABLE I. Top 30 low-lying isomers of C_{24} (in DMOL3 energy ranking). The geometries are optimized (using DMOL3) without symmetry constraint. Energies are in units of eV. The four-member rings (4-MRs) and three-member ring are highlighted in dark grey.

No.	E_{Dmol3}[a]	Sym.[b]	Structure	No.	E_{Dmol3}	Sym.	Structure	No.	E_{Dmol3}	Sym.	Structure
1)	0.00	C_{6v}	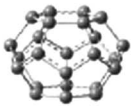	11)	1.02	C_2	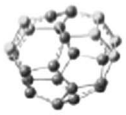	21)	1.53	C_1	
2)	0.09	C_2		12)	1.05	C_1		22)	1.54	C_s	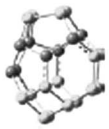
3)	0.10	C_s		13)	1.14	C_{6h}		23)	1.70	C_s	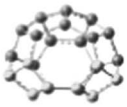
4)	0.15	D_{6h}		14)	1.15	D_{2h}		24)	1.74	C_s	
5)	0.24	C_s	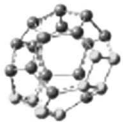	15)	1.28	C_s	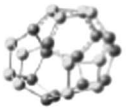	25)	1.78	C_1	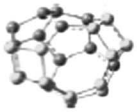
6)	0.54	C_1	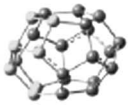	16)	1.34	C_1	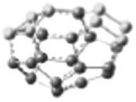	26)	1.79	C_1	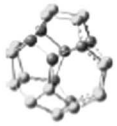
7)	0.56	C_2		17)	1.48	C_1	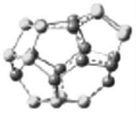	27)	1.88	C_1	
8)	0.60	C_s		18)	1.50	O_h		28)	1.96	C_1	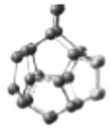
9)	0.71	C_1	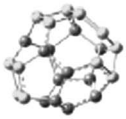	19)	1.52	C_1		29)	2.23	C_s	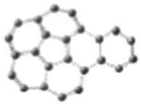
10)	0.97	C_2		20)	1.53	C_1	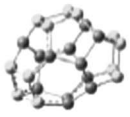	30)	2.30	C_1	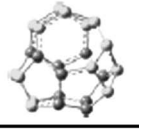

[a]In DMOL3 calculations, PBE functional was used with the DND basis set and a global orbital cutoff radius of 4.0 Å.
[b]Symmetry obtained within a numerical tolerance of 0.1 Å in bond length.

4-MRs satisfy $s+p+h=n/2+2$ and $2s+p=12$ rule,[14] where n denotes the number of carbon atoms, and s, p, and h denote the number of tetragons, pentagons, and hexagons, respectively. D_{6d} is the highest symmetry for 1 but its actual symmetry is lower[22,23] due to the first-order Jahn–Teller distortion. Isomer 6 has the highest possible symmetry D_{24h} but reduced to D_{12h} or C_{12h} (depending on numerical tolerance) symmetry in geometry optimization.[23] Summarizing, the symmetry of optimized isomers 1, 5, and 6 is C_2, D_{6h}, and D_{12h}, respectively.

Unlike the nonclassical fullerene C_{62} whose 4-MR is entirely surrounded by four hexagons, isomer 2 has two 4-MRs surrounded by two alternating hexagons and pentagons, suggesting that hexagons in 2 tend to be adjacent to 4-MRs.

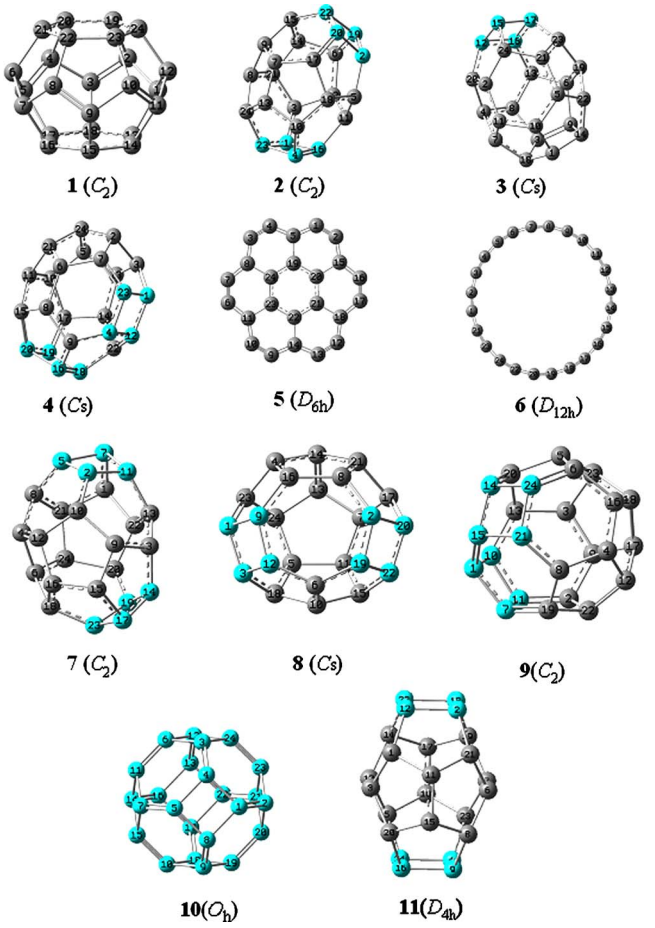

FIG. 1. (Color online) Optimized structures of six low-lying C_{24} isomers. Isomer 1 is a classical fullerene (C_2); 2 a nonclassical fullerene containing two 4-MRs (C_2); 3 a nonclassical fullerene containing one 4-MR (C_s); 4 a nonclassical fullerene containing two 4-MRs (C_s); 5 a plate (D_{6h}); and 6 a monocyclic ring (C_{4h}). Five higher-energy nonclassical fullerene isomers 7–11 are also displayed. The four-membered rings (4-MRs) were highlighted in blue. The figure was prepared using GAUSSVIEW 3.0 program (Ref. 45).

Compared to the classical fullerene 1, the incorporation of two 4-MRs in 2 leads to a gain of two 6-MRs and a loss of four 5-MRs.

Covalent bonds with characters of single, one-and-half, double, and triple bonds are identified in 5, with double and triple bonds in 6, and single, one-and-half, double bonds in 1–4 (see Fig. 1). Partially resonance configurations are expected in these C_{24} isomers for stability reasons. Some similarities between the classical and nonclassical fullerene isomers can be seen concerning the bond lengths and types.

B. Chemical stabilities

Aromaticity is an important indicator of chemical stability for a polycyclic π-electron system. Aromatic molecules are chemically more stable than those less aromatic or antiaromatic molecules because resonance configurations (with delocalized π electrons) are expected to give rise to additional stabilization (cyclic delocalization) in aromatic structures besides the stabilization by conjugation alone. Two-dimensional (2D) monocyclic aromaticity has been well correlated with the Hückel $(4N+2)$ π-electron rule. The Hirsch's $2(N+1)^2$ π-electron rule has also been proposed for three-dimensional (3D) spherical/cylindrical aromaticity.[46,48] Aromatic molecules can sustain diatropic ring currents which bring strong nuclear magnetic shielding effects[57–60] manifested by diamagnetic susceptibility enhancement. For probing aromaticity, NICSs (Ref. 47) have been widely accepted as a reliable indicator.[46–52] The NICS is measured as magnetic shielding at positions with little electron density in a molecule. In general, aromaticity and antiaromaticity are characterized by negative (diamagnetic) and positive (paramagnetic) NICS values, respectively. Larger negative NICS values represent stronger aromaticity.[46–48,59,50–52] For example, the NICS value for D_{6h} planar benzene (satisfying $4N+2$ rule with $N=1$) is -9.7.[47] C_{60}^{10+} fullerene [satisfying the $2(N+1)^2$ rule with $N=4$] exhibits a larger negative NICS value (-78) than that (-2) of C_{60} fullerene [unsatisfying the $2(N+1)^2$ rule].[61] The NICS value can be dependent on the level of theory, as shown by NICS of C_{60}.[47] It appears that the NICS value is a better aromaticity indicator when comparing molecules with similar topology.

The NICS values can be used to correlate with measured NMR chemical shifts of endohedral atoms. For example, NICS versus ^{3}He NMR endohedral chemical shift for $^3He@C_{60}$, $^3He@C_{60}^{6-}$, and $^3He@C_{70}$ are -8.5 versus -6.4 ppm, -64.4 versus -49.3 ppm, and -9.3 versus -28.8 ppm, respectively.[52,62–65] Exceptions, however, often occur as noted above by examples of C_{60}^{6-} and C_{70} which do not satisfy the $2(N+1)^2$ rule.

The NICS values of the six low-lying C_{24} isomers were calculated using GIAO method (Table II). Isomers 2–4 have negative NICS values of -19, -14, and -9, respectively, measured at the center of each isomer. In contrast, the classical fullerene isomer 1 has a positive NICS value (42). The NICS in the cage structures is attributed to the balance between dia- and paratropic ring currents localized in the individual 6-MR (diatropic) and 4- or 5-MR (paratropic),[47,52,57–60] and the current gives rise to negative and positive NICS, respectively. The structural changes arising from incorporation of the 4-MRs into a fullerene cage can affect the weight of dia- and paratropic contributions (Table III).

The plate isomer 5, which is a fragment of graphene sheet, comprises seven 6-MRs. The seven 6-MRs are expected to give more diatropic contributions than a single hexagon. However, isomer 5 is actually less aromatic (NICS: -2) than a single hexagon (NICS: -39) as indicated by their NICS values. These results show that the NICS for 2D polycyclic molecules is not simply a sum of diatropical and paratropical contributions from monocyclic ring. It should be noted that since π electrons of C_{24} satisfy neither the $4N+2$ nor $2(N+1)^2$ aromaticity rule, and the cluster itself is expected to exhibit antiaromaticity, evidently in isomers 1 and 6 (NICS: 19) as both have positive NICS values. To some extent, isomer 5 may also exhibit antiaromaticity because of its small negative NICS value. However, nonclassical fullerenes 2–4 all exhibit large negative NICS values, significantly deviating from the antiaromaticity behavior.

To further study geometric effect on NICS, we calculated NICS for monocyclic carbon rings C_n $(6 \leqslant n \leqslant 22)$ and

TABLE II. Point-group symmetry, relative energies (ΔE), singlet-triplet splitting (ΔE_{ST}), electron affinity (EA), ionization potential (IP), HOMO-LUMO gap (E_{gap}), GIAO-NICS, HOMO/LUMO configuration, and electronic state of neutral C_{24} isomers at singlet state. Relative energies [ΔE] and vertical detachment energies [VDE] for anions are also included. Energies and HOMO-LUMO gaps are in units of eV and NICS in ppm.

Isomer	1	2	3	4	5	6
Symmetry[a]	C_2	C_2	C_s	C_s	D_{6h}	D_{12h}
ΔE	0.00	−0.11	0.10	0.07	0.32	2.52
ΔE_{ZPE}[b]	0.00	−0.08	0.09	0.09	0.08	1.95
ΔE_{MP2}[c]	0.00	−0.40	0.11	−0.18	−0.06	⋯
ΔE_{ST}	0.10	0.92	0.30	0.40	2.63	0.96
IP	7.37	7.70	7.37	7.35	8.19	7.27
E_{gap}	2.08	2.83	2.23	2.53	3.94	2.26
NICS	42	−19	−14	−9	−2	19
HOMO/LUMO	$(B)^2/(B)^0$	B^2/B^0	$(A'')^2/(A')^0$	$(A')^2/(A'')^0$	$(E_{2u})^4/(A_{2g})^0$	$(A_g)^2/(A_u)^0$
Electronic State	^1A	^1A	$^1A'$	$^1A'$	$^1A_{1G}$	^1A_G
$[\Delta E_{anion}]$[d]	[0.00]	[0.44]	[0.14]	[0.42]	[1.29]	[2.29]
$[VDE]_{anion}$	[3.43]	[2.53]	[2.83]	[2.81]	[1.97]	[3.20]
EA	3.00	2.45	2.67	2.63	1.89	3.19

[a]Symmetry obtained within a numerical tolerance of 0.001 Å and based on geometries optimized at PBE1PBE/cc-pVTZ level.
[b]Relative energies including zero-point energy (ZPE) corrections calculated at the PBE1PBE/cc-pVTZ level.
[c]Calculated at the MP2/cc-pVTZ//PBE1PBE/cc-pVTZ level.
[d]Calculated at the PBE1PBE/cc-pVTZ level.

benzene using the PBE1PBE/cc-pVTZ level of theory (Table IV). We found that C_6 hexagon and benzene shows a large difference in NICS, i.e. −39 versus −8 ppm, although both molecules have the same number of π electrons and both satisfy the $4N+2$ rule with $N=1$. Apparently, the larger negative NICS for the C_6 hexagon is attributed to unconstrained dangling bonds (σ electrons), leading to certain σ-aromatic characteristics in the C_6 hexagon. To summarize, as far as the NICS value of a molecule is concerned, contributions from local circulations of electrons in σ-bonds, in lone pairs, and even in atom cores should not be ignored.[48,49] These non-π-electron contributions to NICS can explain anomalous trend in NICS, which disobeys the Hückel and Hirsch's rules.

The C_{10} ($N=2$), C_{18} ($N=4$), and C_{22} ($N=5$) monocyclic rings with $4N+2$ π electrons yield nearly the same negative NICS values (−42, −43, and −43, respectively), indicating that magnetic shielding at the center of C_{4N+2} monocyclic ring remain invariant with increasing N ($1<N\leqslant 5$), in contrast to $4N+2$ π-electron $C_{4N+2}H_{4N+2}$ annulenes.[47] Moreover, bond-length and bond-angle variations were not seen within these C_{4N+2} rings ($1<N\leqslant 5$), consistent with the fact that highly aromatic systems with closed-shell annulenelike structures tend to retain the highest possible D_{nh} symmetry. Still, C_{22} ($N=5$) with D_{22h} symmetry (measured with high numerical tolerance, see Table IV) appears to be a transition state ($-816.2i$ cm^{-1}), suggesting that the Jahn–Teller effect becomes increasingly important for C_{4N+2} rings with $N\geqslant 5$.[66] Moreover, positive NICS values are obtained for C_{4N} monocyclic rings, such as NICS=26 for C_{20} ($N=5$) and 19 for C_{24} ($N=6$). In these C_{4N} rings, bond variations can arise from both antiaromaticity and Jahn–Teller effect (Table IV).

Although NICS at cage center may not always correlate with the aromaticity,[48] a negative NICS value still represents diatropicity at the cage center, a manifestation of overall diamagnetic currents circulating around the fullerene cages.[57–60] Because negative (positive) NICS value often correlates with large (small) highest occupied molecular orbital–lowest unoccupied molecular orbital (HOMO-LUMO) gap (Table II), endohedral NICS may be used as an indicator for analyzing relative chemical stability of fullerenes. To gain more insight into the diatropicity of nonclassical fullerene and paratropicity of classical fullerene, we undertook a more detailed analyses of individual MO-NICS (method is given in Refs. 49–51) for 1 and 2 using both GIAO and CMO methods (Table III). The incorporations of 4-MRs into the cage considerably reduce paratropic contributions from HOMO, HOMO-1, and HOMO-2, which are mainly responsible for the sign change in NICS from positive for isomer 1 to negative for isomer 2. The NICS is primarily contributed by the π-electrons as validated by $4N+2$ and $2(N+1)^2$ rules. A 3D π-electron system such as fullerene may be also viewed as a spherical electron gas surrounding the surface of a sphere.[46] As such, the σ-framework of the fullerene cage should be taken into account, as shown by the MO-NICS analyses.

The energy splitting (ΔE_{ST}) between the singlet and triplet states at their corresponding optimized geometry is another index for analyzing chemical stabilities.[21] The third index is the HOMO-LUMO gap (E_{gap}). A fullerene with a large E_{gap} and IP tends to exhibit low chemical reactivity. For example, fullerene C_{60} is known to be very stable since it has a large E_{gap} of 1.57 ± 0.03 eV (Ref. 67) and IP of 7.54 ± 0.04 eV (Ref. 68). Isomer 2 has the largest ΔE_{ST}, E_{gap}, and IP among the four cage isomers (Table II). The large values of ΔE_{ST} and E_{gap} of isomer 2 correlate well with its relatively smaller electron affinity (EA) and larger IP compared to cage isomers 1, 3, and 4. The EA value of the monocyclic ring 6 may be overestimated by DFT.[26]

Finally, the total-energy calculation at the PBE1PBE/cc-pVTZ and MP2/cc-pVTZ//PBE1PBE/cc-pVTZ levels of

TABLE III. Comparison of NBO-NLMO-NICS (GIAO) and NBO-CMO-NICS (CMO) between isomers 1 and 2. The calculation was performed at the PBE1PBE/cc-pVTZ level of theory. The paratropical contributions are highlighted in boldface.

NLMO (label)	Isomer 1 MO-NICS[a]	NLMO (label)	Isomer 2 MO-NICS	CMO (label)	Isomer 1 MO-NICS[a]	CMO (label)	Isomer 2 MO-NICS
2(B)	−1.79	1(A)	−1.05	25(A)	−7.55	25(A)	−7.35
3(A)	**9.35**	6(B)	−1.17	26(B)	−7.15	26(B)	−6.75
5(B)	−1.80	**7(B)**	**1.45**	27(B)	−7.14	27(B)	−6.97
6(A)	**8.88**	12(A)	−1.17	28(A)	−6.84	28(A)	−6.84
10(B)	−1.79	**13(B)**	**1.45**	29(A)	−6.57	29(A)	−6.35
11(A)	**9.22**	15(B)	−1.49	30(A)	−6.55	30(A)	−6.03
15(B)	−1.80	16(A)	−1.51	31(B)	−5.83	31(B)	−5.75
16(A)	**8.63**	18(A)	−1.20	32(B)	−5.81	32(A)	−5.80
20(A)	−1.79	19(B)	−1.22	33(A)	−5.60	33(B)	−6.03
21(A)	**9.12**	22(A)	−1.54	34(B)	−4.22	34(B)	−4.35
25(A)	−1.79	24(A)	−1.04	35(B)	−2.65	35(A)	−3.51
26(B)	**8.70**	26(B)	−1.27	36(B)	−2.13	36(B)	−3.94
31(B)	−1.47	27(B)	−1.54	37(B)	−4.57	37(B)	−3.94
32(B)	−1.54	31(B)	−1.22	38(A)	−5.36	38(A)	−2.52
33(A)	**3.34**	33(B)	−1.20	39(A)	−5.37	39(B)	−6.44
34(B)	−1.53	34(B)	−1.51	40(A)	−7.47	40(A)	−4.98
35(B)	**2.28**	39(B)	−1.04	41(A)	−1.92	41(A)	−3.87
38(A)	**2.90**	**41(A)**	**3.22**	42(A)	−1.90	42(B)	−2.87
39(A)	−1.48	43(A)	−1.05	43(A)	−1.01	43(A)	−1.01
40(A)	−1.53	**48(B)**	**3.22**	45(B)	−3.20	44(B)	−1.05
41(A)	**2.75**	Sum	−19.21	46(B)	−3.00	45(A)	−2.77
42(A)	−1.46			47(B)	−1.71	46(A)	−1.41
43(A)	−1.49			48(B)	−1.69	47(A)	−7.45
44(A)	−1.52			49(A)	−7.44	48(B)	−1.04
45(B)	**1.94**			50(A)	−2.81	50(B)	−1.39
46(B)	−1.47			51(B)	−1.97	**52(B)**	**1.88**
47(B)	−1.53			52(B)	−2.16	**53(A)**	**2.95**
48(B)	**3.66**			**53(B)**	**6.81**	54(B)	−2.28
Sum	41.99			**54(B)**	**6.86**	55(B)	−3.15
				57(A)	−5.46	**56(A)**	**6.13**
				58(A)	**9.35**	57(A)	−2.67
				59(A)	**9.31**	**58(B)**	**3.59**
				60(B)	**9.73**	**59(A)**	**7.69**
				61(B)	**9.67**	**60(B)**	**7.41**
				62(A)	**8.59**	**61(A)**	**8.55**
				63(A)	**8.52**	**62(A)**	**11.77**
				64(A)	**14.11**	63(A)	−1.16
				65(A)	−2.51	**64(B)**	**9.00**
				66(A)	−2.57	**65(A)**	**11.55**
				67(B)	−1.95	**70(B)**	**10.60**
				68(B)	−1.94	**71(A)**	**21.88**
				70(B)	**54.59**	**72(B)**	**13.19**
				71(B)	**27.70**	Sum	−19.21
				72(B)	**27.93**		
				Sum	41.99		

[a]Only MO-NICS $\geqslant$ 1.00 ppm are listed.

theory suggests that isomer 2 has the lowest energy, 0.11 (0.08 eV if including zero-point energy correction) and 0.40 eV lower in energy than isomer 1, respectively. Although high-level *ab initio* methods, e.g., coupled-cluster calculation with a large basis set (e.g., cc-pVTZ), are required to determine the true global minimum of C_{24}, it is still reasonable to conclude that nonclassical fullerene with 4-MRs can be energetically competitive compared to the classical fullerene, at the least for C_{24}.

C. Anion photoelectron spectroscopy

Anion PES is a valuable tool to measure electronic properties of clusters. Distinct spectral features can be useful as an electronic fingerprint to distinguish isomer's identity. The experimental photoelectron spectra of carbon clusters C_n^- in the size of $n=2-29$ and 44, 60, and 70 have been reported.[8,13,28,30,67,68] However, determination of the C_n^- structures based on the measured PES spectra is a challenging task especially for small-sized C_n^- clusters. This is largely

TABLE IV. Geometry and GIAO-NICS for monocyclic-ring structures of C_{4N+2} and C_{4N}.

	$(4N+2)$ π system					$(4N)$ π system	
Ring size	Benzene	C_6	C_{10}	C_{18}	C_{22}	C_{20}	C_{24}
(N)	(1)	(1)	(2)	(4)	(5)	(5)	(6)
Symmetry[a]	(D_{6h})	(D_{6h})	(D_{10h})	(D_{18h})	(D_{22h})[b]	(D_{10h})[b]	(D_{12h})
Bond length	1.388	1.299	1.281	1.276	1.275	1.341	1.226
(Å)						1.225	1.337
Bond angle (deg)	120.0	120.0	144.0	160.0	163.7	162.0	165.0
NICS (ppm)	−8	−39	−42	−43	−43	26	19

[a]Symmetry obtained with a numerical tolerance of 0.001 Å.
[b]Symmetry obtained with a numerical tolerance of 0.05 Å.

because coexistence of several low-lying isomers renders producing a sole ground-state structure impossible under experimental conditions.

For C_{24}^-, mono- and bicyclic ring structures were previously identified to interpret the measured PES features.[28,30] A tadpole structure (a monocyclic ring attached by a small linear chain) was also assigned according to high-resolution ion-mobility measurement.[69] We calculated the simulated photoelectron spectra (Figs. 2 and 3) of the six C_{24}^- isomers (1–6), as well as that of a tadpole (the most stable tadpole structure suggested in Ref. 69) and three typical bicyclic-ring structures, considering the binding energy up to 6.5 eV. The simulated photoelectron spectra are based on ground-state transition in which electrons are photodetached from doublet state of anion to ground state of neutral without geometry relaxation (Franck–Condon effect). Only optimized geometries of C_{24}^- were used in calculating vertical detachment energies. In experimental PES, the adiabatic detachment energy (ADE) and vertical detachment energy (VDE) corresponds to the onset and the maximum position of the first peak in the spectra, respectively. The separation between the first and second peaks is related to HOMO-LUMO gap (E_{gap}) of the neutral. Accordingly, the position of ADE can be approximated as EA for the neutral counterpart, which is theoretically defined as $EA = E_{ZPE}^{neutral}$ (optimized neutral geometry) $- E_{ZPE}^{anion}$ (optimized anion geometry).[70] Calculated EAs are collected in Table II. The calculated EAs for neutral C_{24} isomers are consistent with the anion spectral features.

The simulated PES spectra of 1–4 exhibit certain similarities due to geometry similarities in these clusters. The simulated PES for mono- and bicyclic rings (with C_1 symmetry) exhibit a large HOMO-LUMO gap of ~1 eV [see Fig. 2(a) (isomer 6) and Fig. 3 (C_1 isomer)], which matches the measured gap quite well [for comparison, experimental PES spectra[28] are plotted in Fig. 2(b)]. However, the calculated VDEs of isomer 3 (2.83 eV) and 4 (2.81 eV) also match the experimental VDE (2.9 eV) very well, even better than the VDEs (3.20 eV for 6 and 3.10 eV for the bicyclic ring with C_1 symmetry) of ringlike structures. Moreover, the first and second bands in experimental spectra [Fig. 2(b)][28,71] are very broad, suggesting existence of multiple isomers other than the mono- and bicyclic ring isomers (see Fig. 3). We conclude that the cage isomers 3 and 4 are two possible candidates to be coexistent with the mono- and bicyclic ring isomers in the cluster beam.

It is also worthy to mention that a recent PES measurement[13] of C_{20} fullerene has been reported. Here, we replot the simulated anion PES spectrum for C_{20} fullerene

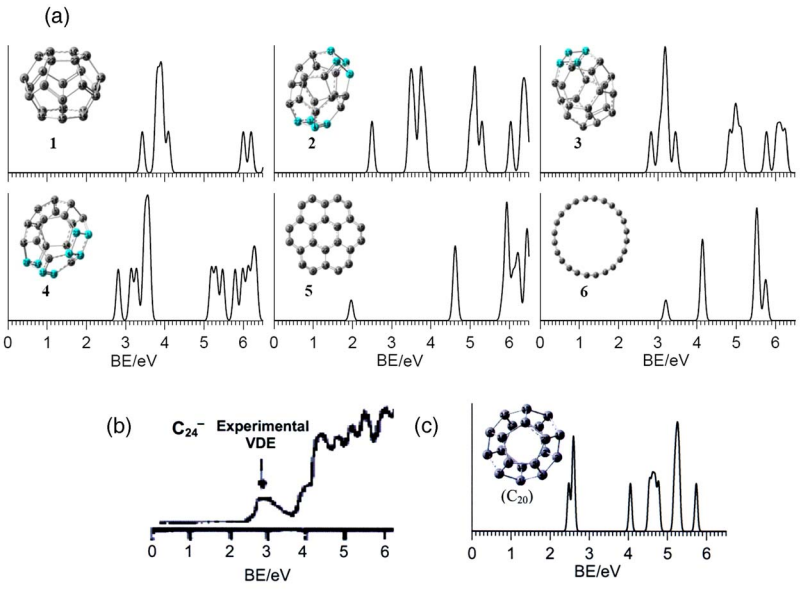

FIG. 2. (Color online) (a) Simulated anion photoelectron spectra for the six low-lying C_{24}^- isomers. The spectra were constructed by fitting each of the vertical detachment transitions with a gaussian broadening of 0.05 eV. (b) A plot of measured PES spectrum (originally reported in Ref. 28) of C_{24}^-. (c) Simulated anion photoelectron spectrum of C_{20}^- fullerene isomer for comparison with measured PES spectrum (Ref. 13).

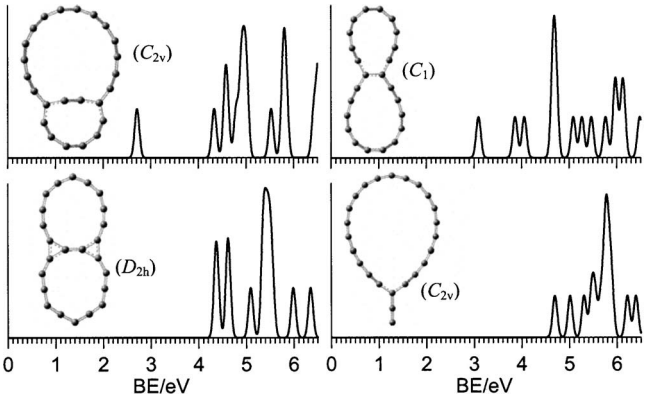

FIG. 3. Simulated anion photoelectron spectra for one tadpole and three typical bicyclic ring C_{24}^- isomers. The spectra were constructed by fitting each of the vertical detachment transitions with a Gaussian broadening of 0.05 eV.

[Fig. 2(c)]. We find both calculated VDE (2.48 eV) and simulated spectral features agree quite well with the measured spectra, suggesting that the method we used to calculate PES spectra is reasonable, at least for small-sized carbon cluster.

D. Thermal Stabilities

Figure 4 shows that the 2D anion isomers (5 and 6) are increasingly stable than the cage structures (1–4) as the temperature is increased, a manifestation of strong entropy effect at elevated temperatures. Beyond 700 K, the monocyclic ring isomer becomes the most stable isomer. This explains why the ringlike structures are the most populated isomers of C_{24}^- under the PES experimental conditions.[28,30,71] At elevated temperatures, cage isomer 1 is more stable than 2–4 (Fig. 4). However, as shown in Fig. 2(a) (isomer 1), the VDE

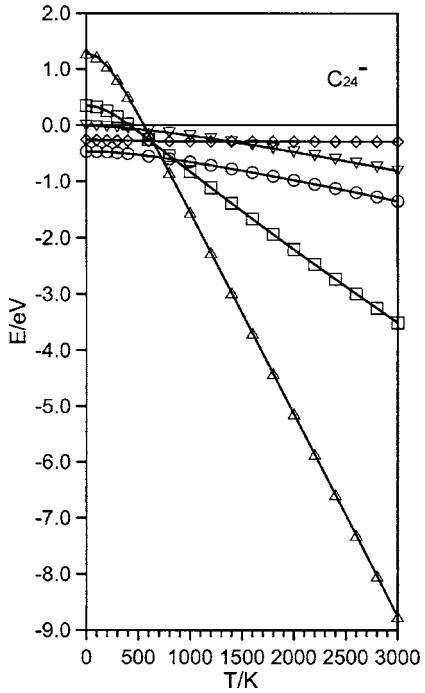

FIG. 4. Relative Gibbs free energy as a function of temperature for C_{24}^- isomers: 2 (0-eV line), 1 (○), 3 (◇), 4 (▽), 5 (□), and 6 (△).

of anion isomer 1 (3.43 eV) does not match the measured VDE [2.9 eV, see Fig. 2(b)] well. Hence, one may rule out the existence of classical fullerene 1 under the experimental conditions.

IV. CONCLUSIONS

Incorporation of 4-MRs into a fullerene cage can overcome certain pentagon-adjacency penalty. As a result, some nonclassical fullerenes can be energetically as competitive as their classical fullerene counterpart. Structural changes due to the 4-MR insertion can affect both chemical and electronic properties of C_{24} clusters. Calculations of NICS, singlet-triplet splitting, IP, and HOMO-LUMO gap at DFT level all indicate that the neutral isomer 2 of C_{24}, a nonclassical fullerene containing two 4-MRs, is superior in chemical stability to the classical fullerene isomer 1. Although C_{24} satisfies neither the $4N+2$ nor $2(N+1)^2$ aromaticity rule, negative NICS values are found for all three nonclassical fullerene isomers 2–4. The negative NICS values are mainly attributed to the reduction of paratropic contributions from HOMO, HOMO-1, and HOMO-2, as shown from the MO-NICS analysis for 1 and 2. It appears that relative stabilities of cage isomers are dependent on a subtle competition between the steric σ-strain and electronic π-bonding delocalization effects.

Finally, the simulated PES spectra for various C_{24}^- isomers display distinct spectral features. Among them, nonclassical fullerene isomers 3 and 4 match the measured VDE reasonably well, whereas the mono- and bicyclic rings match the measured HOMO-LUMO gap very well. Because the first and second bands in experimental spectra are very broad,[28,30,71] it is likely that there exist multiple isomers in addition to the mono- and bicyclic ring isomers in the cluster beam. Our results suggest that 3 and 4 are two conceivable cage isomers coexisting with the mono- and bicyclic ring isomers in the cluster beam under the PES experimental conditions.

ACKNOWLEDGMENTS

We are grateful of valuable discussions with Professor L.-S. Wang and L.-M. Wang. This research was supported in part by grants from DOE (DE-FG02-04ER46164), NSF (CHE-0427746 and CHE-0701540), and the Nebraska Research Initiative, and by the Research Computing Facility at University of Nebraska-Lincoln.

[1] H. W. Kroto, J. R. Heath, S. C. O'Brien, R. F. Curl, and R. E. Smalley, Nature (London) **318**, 162 (1985).
[2] W. Krätschmer, L. D. Lamb, K. Fostiropoulos, and D. R. Huffman, Nature (London) **347**, 354 (1990).
[3] P. W. Fowler and D. E. Manolopoulos, Nature (London) **355**, 428 (1992).
[4] H. W. Kroto, Nature (London) **329**, 529 (1987).
[5] T. G. Schmalz, W. A. Seitz, D. J. Klein, and G. E. Hite, J. Am. Chem. Soc. **110**, 1113 (1988).
[6] R. E. Haufler, Y. Chai, L. P. F. Chibante, J. Concicao, C. Jin, L.-S. Wang, S. Maruyama, and R. E. Smalley, *MRS Symposia Proceedings* No. 206 (Materials Research Society, Pittsburgh, 1991), p. 627.
[7] M. F. Jarrold, Nature (London) **407**, 26 (2000).
[8] H. Prinzbach, A. Weiler, P. Landenberger, F. Wahl, J. Wörth, L. T. Scott, M. Gelmont, D. Olevano, and B. v. Issendorff, Nature (London) **407**, 60 (2000).

[9] C. Piskoti, J. Yarger, and A. Zettl, Nature (London) **393**, 771 (1998).
[10] R. Ettl, I. Chao, F. Diederich, and R. L. Whetten, Nature (London) **353**, 149 (1991).
[11] J. Weaver, J. Martins, T. Komeda, Y. Chen, T. R. Ohno, G. Kroll, N. Troullier, E. Haufler, and R. Smalley, Phys. Rev. Lett. **66**, 1741 (1991).
[12] Y. Yang, F. Arias, L. Echegoyen, L. P. Felipe Chibante, S. Flanagan, A. Robertson, and L. J. Wilson, J. Am. Chem. Soc. **117**, 7801 (1995).
[13] H. Prinzbach, F. Wahl, A. Weiler, P. Landenberger, J. Wörth, L. T. Scott, M. Gelmont, D. Olevano, F. Sommer, and B. von Issendorff, Chem.-Eur. J. **12**, 6268 (2006).
[14] P. W. Fowler, T. Heine, D. E. Manolopoulos, D. Mitchell, G. Orlandi, R. Schmidt, G. Seifert, and F. Zerbetto, J. Phys. Chem. **100**, 6984 (1996).
[15] E. Albertazzi, C. Domene, P. W. Fowler, T. Heine, G. Seifert, C. Van Alsenoy, and F. Zerbetto, Phys. Chem. Chem. Phys. **1**, 2913 (1999).
[16] D. Babić and N. Trinajstić, Chem. Phys. Lett. **237**, 239 (1995).
[17] R. O. Jones and G. Seifert, Phys. Rev. Lett. **79**, 443 (1997).
[18] M. C. Domene, P. W. Fowler, D. Mitchell, G. Seifert, and F. Zerbetto, J. Phys. Chem. **101**, 8339 (1997).
[19] S. Stevenson, P. W. Fowler, T. Heine, J. C. Duchamp, G. Rice, T. Glass, K. Harich, E. Hajdu, R. Bible, and H. C. Dorn, Nature (London) **408**, 427 (2000).
[20] S. Diaz-Tendero, F. Martin, and M. Alcami, ChemPhysChem **6**, 92 (2005).
[21] W. Y. Qian, M. D. Bartberger, S. J. Pastor, K. N. Houk, C. L. Wilkins, and Y. Rubin, J. Am. Chem. Soc. **122**, 8333 (2000); W. Y. Qian, S.-C. Chuang, R. B. Amador, T. Jarrosson, M. Sander, S. Pieniazek, S. I. Khan, and Y. Rubin, *ibid.* **125**, 2066 (2003).
[22] B. Paulus, Phys. Chem. Chem. Phys. **5**, 3364 (2003).
[23] F. Jensen and H. Koch, J. Chem. Phys. **108**, 3213 (1998).
[24] M. Feyereisen, M. Gutowski, J. Simons, and J. Almlöf, J. Chem. Phys. **96**, 2926 (1992).
[25] K. Raghavachari, B. Zhang, J. A. Pople, B. G. Johnson, and P. M. W. Gill, Chem. Phys. Lett. **220**, 385 (1994).
[26] W. An, Y. Gao, S. Bulusu, and X. C. Zeng, J. Chem. Phys. **122**, 204109 (2005).
[27] C. Zhang, W. Sun, and Z. Cao, J. Chem. Phys. **126**, 144306 (2007).
[28] S. Yang, K. J. Taylor, M. J. Craycraft, J. Conceico, O. Cheshnovsky, and R. E. Smalley, Chem. Phys. Lett. **144**, 431 (1988).
[29] H. Kietzmann, R. Rochow, G. Ganteför, W. Eberhardt, K. Vietze, G. Seifert, and P. W. Fowler, Phys. Rev. Lett. **81**, 5378 (1998).
[30] H. Handschuh, G. Ganteför, B. Kessler, P. S. Bechthold, and W. Eberhardt, Phys. Rev. Lett. **74**, 1095 (1995).
[31] S. Diaz-Tendero, G. Sanchez, M. Alcami, and F. Martin, Int. J. Mass. Spectrom. **252**, 133 (2006).
[32] R. E. Smalley, Acc. Chem. Res. **25**, 98 (1992).
[33] G. von Helden, N. G. Gotts, and M. T. Bowers, Nature (London) **363**, 60 (1993).
[34] H. W. Kroto and K. McKay, Nature (London) **331**, 328 (1988).
[35] G. E. Scuseria, Science **271**, 942 (1996).
[36] J. M. Hunter, J. L. Fye, E. J. Roskamp, and M. F. Jarrold, J. Phys. Chem. **98**, 1810 (1994).
[37] S. Irle, G. Zheng, Z. Wang, and K. Morokuma, J. Phys. Chem. B **110**, 14531 (2006).
[38] V. V. Pokropivny and A. V. Pokropivny, Phys. Solid State **46**, 392 (2004).
[39] D. J. Wales, *Energy Landscapes-With Applications to Clusters, Biomolecules and Glasses* (Cambridge University, Cambridge, 2003).
[40] B. Delley, J. Chem. Phys. **92**, 508 (1990); **113**, 7756 (2000).
[41] J. Hutter, A. Alavi, T. Deutsch, M. Bernasconi, S. Goedecker, D. Marx, M. Tuckerman, and M. Parrinello, CPMD, Version 3.7.1, MPI für Festkörperforschung Stuttgart, 1997–2001 (http://www.cpmd.org/).
[42] S. Yoo and X. C. Zeng, Angew. Chem., Int. Ed. **44**, 1491 (2005).
[43] J. P. Perdew, K. Burke, and M. Ernzerhof, Phys. Rev. Lett. **77**, 3865 (1996); **78**, 1396 (1997).
[44] T. H. Dunning, Jr., J. Chem. Phys. **90**, 1007 (1989).
[45] M. J. Frisch, G. W. Trucks, H. B. Schlegel *et al.*, GAUSSIAN, Gaussian, Inc., Wallingford, CT, 2004; GAUSSVIEW 3.0, Gaussian, Inc., Pittsburgh, PA, 2002.
[46] A. Hirsch, Z. Chen, and H. Jiao, Angew. Chem., Int. Ed. **39**, 3915 (2000); M. Bühl and A. Hirsch, Chem. Rev. (Washington, D.C.) **101**, 1153 (2001).
[47] P. von R. Schleyer, C. Maerker, A. Dransfeld, H. Jiao, and N. J. R. van Eikema Hommes, J. Am. Chem. Soc. **118**, 6317 (1996).
[48] J. Aihara and T. Tamaribuchi, Chem. Phys. Lett. **374**, 104 (2003).
[49] T. Heine, P. Schleyer, C. Corminboeuf, G. Seifert, R. Reviakine, and J. Weber, J. Phys. Chem. A **107**, 6470 (2003).
[50] C. S. Wannere, C. Corminboeuf, Z.-X. Wang, M. D. Wodrich, R. B. King, and P. Schleyer, J. Am. Chem. Soc. **127**, 5701 (2005).
[51] R. B. King, T. Heine, C. Corminboeuf, and P. Schleyer, J. Am. Chem. Soc. **126**, 430 (2004).
[52] M. Bühl, Chem.-Eur. J. **4**, 734 (1998).
[53] R. Ditchfield, Mol. Phys. **27**, 789 (1974).
[54] K. Wolinski, J. F. Hinton, and P. Pulay, J. Am. Chem. Soc. **112**, 8251 (1990).
[55] J. A. Bohmann, F. Weinhold, and T. C. Tarrar, J. Chem. Phys. **107**, 1173 (1997).
[56] E. D. Glendening, J. K. Badenhoop, A. E. Reed, J. E. Carpenter, J. A. Bohmann, C. M. Morales, and F. Weinhold, NBO 5.0, Theoretical Chemistry Institute, University of Wisconsin, Madison, WI, 2001 (http://www.chem.wisc.edu/~nbo5).
[57] A. Pasquarello, M. Schlüter, and R. C. Haddon, Science **257**, 1660 (1992).
[58] R. C. Haddon, Nature (London) **378**, 249 (1995).
[59] M. Prato, T. Suzuki, F. Wudl, V. Lucchini, and M. Maggini, J. Am. Chem. Soc. **115**, 7876 (1993).
[60] A. Pasquarello, M. Schlüter, and R. C. Haddon, Phys. Rev. A **47**, 1783 (1993).
[61] M. P. Johansson, D. Sundholm, and J. Vaara, Angew. Chem., Int. Ed. **43**, 2678 (2004).
[62] E. Shabtai, A. Weitz, R. C. Haddon, R. E. Hoffman, M. Rabinovitz, A. Khong, R. J. Cross, M. Saunders, P.-C. Cheng, and L. T. Scott, J. Am. Chem. Soc. **120**, 6389 (1998).
[63] T. Sternfeld, R. E. Hoffman, M. Saunders, R. J. Cross, M. S. Syamala, and M. Rabinovitz, J. Am. Chem. Soc. **124**, 8786 (2002).
[64] M. Saunders, H. A. Jiménez-Vázquez, R. J. Cross, S. Mroczkowski, D. I. Freedberg, and F. A. L. Anet, Nature (London) **367**, 256 (1994).
[65] M. Buhl, W. Thiel, H. Jiao, P. von R. Schleyer, M. Saunders, and F. A. L. Anet, J. Am. Chem. Soc. **116**, 6005 (1998).
[66] M. Saito and Y. Okamoto, Phys. Rev. B **60**, 8939 (1999).
[67] X.-B. Wang, C.-F. Ding, and L. S. Wang, J. Chem. Phys. **110**, 8217 (1999).
[68] I. V. Hertel, H. Steger, J. de Vries, B. Weisser, C. Menzel, B. Kamke, and W. Kamke, Phys. Rev. Lett. **68**, 784 (1992).
[69] P. Dugourd, R. R. Hudgins, J. M. Tenenbaum, and M. F. Jarrold, Phys. Rev. Lett. **80**, 4197 (1998).
[70] J. C. Rienstra-Kiracofe, G. S. Tschumper, and H. F. Schaefer III, Chem. Rev. (Washington, D.C.) **102**, 231 (2002).
[71] L.-M. Wang and L.-S. Wang (unpublished).